The curled wake model: A three-dimensional and extremely fast steady-state wake solver for wind plant flows

Luis A Martínez-Tossas[1], Jennifer King[1], Eliot Quon[1], Christopher J Bay[1], Rafael Mudafort[1], Nicholas Hamilton[1], and Paul Fleming[1]

[1]National Renewable Energy Laboratory, Golden, CO USA

Correspondence: luis.martinez@nrel.gov

Abstract. This work focuses on minimizing the computational cost of steady-state wind power plant flow simulations that take into account wake steering physics. We present a simple wake solver with a computational cost on the order of seconds for large wind plants. The solver uses a simplified form of the Reynolds-averaged Navier-Stokes equations to obtain a parabolic equation for the wake deficit of a wind plant. We compare results from the model to supervisory control and data acquisition (SCADA) from the Lillgrund wind plant; good agreement is obtained. Results for the solver in complex terrain are also shown. Finally, the solver is demonstrated for a case with wake steering showing good agreement with power reported by large-eddy simulations. This new solver minimizes the time–and therefore the related cost–it takes to conduct a steady-state wind plant flow simulation to about a second on a personal laptop. This solver can be used for different applications including wake steering for wind power plants and layout optimization, and it will soon be available within the FLOw Redirection and Induction in Steady State (FLORIS) framework.

1 Introduction

In this work, we present an improved formulation of the curled wake model (Martínez-Tossas et al., 2019) that can be used in the context of a wind power plant without the need to use a wake superposition method. Wake superposition models are typically used because of their computational efficiency; however, they have been shown to give different results depending on the model used (Gunn et al., 2016; Zong and Porté-Agel, 2020). This inconsistency motivates the use of a more robust solver in the context of the curled wake model (Martínez-Tossas et al., 2019) that does not depend on a superposition method. The new solver is developed by simplifying the Reynolds-averaged Navier-Stokes (RANS) equations to obtain a parabolic equation for the wake deficit. The equation is solved in a three-dimensional domain to obtain the wake velocity in a wind plant.

Parabolic solvers for RANS equations are a promising tool for fast wind farm flow solvers. Other researchers have developed parabolic solvers for wind plant applications. Iungo et al. (2018) developed a parabolic RANS solver focused on improving the mixing-length model and used assumptions about axisymmetry in the wakes. Bradstock and Schlez (2019a, b) have developed a parabolic wind plant RANS solver (WakeBlaster) used for commercial applications. WakeBlaster solves a simplified version of the RANS equations and has been validated using field experiments. WakeBlaster uses a special method to solve the spanwise velocity components that does not include effects caused by yaw. The curled wake solver presented in this work focuses on

minimizing computational cost and capturing wake steering effects. This is done by solving only the streamwise component of the linearized RANS equations and parametrizing the effects of the spanwise and wall-normal components using semianalytical solutions.

Wake steering is a promising wind plant control strategy used to maximize the power output of a wind plant (Adaramola and Krogstad, 2011; Park et al., 2013; Gebraad et al., 2016; Howland et al., 2019; Fleming et al., 2019; Siemens Gamesa, 2019). In wake steering, upstream turbines are yawed, deflecting the wakes such that downstream turbines are able to produce more power, and the wind plant as a whole can produce more power. In this work, we present a wind plant model that uses a simplified version of the RANS equations to predict the flow through a wind plant with wake steering. This tool is extremely fast (order of seconds), thereby enabling controls-oriented frameworks used for wind plant operation and layout optimization.

The wake of a wind turbine in yaw has a unique shape known as the curled wake (Howland et al., 2016; Bastankhah and Porté-Agel, 2016; Martínez-Tossas et al., 2019). This shape has been observed in computational fluid dynamics simulations and in small- and large-scale experiments (Medici and Alfredsson, 2006; Howland et al., 2016; Bastankhah and Porté-Agel, 2016; Vollmer et al., 2016; Bartl et al., 2018; Fleming et al., 2018b; Schottler et al., 2018). The curled wake is formed because the wake of a wind turbine in yaw introduces spanwise and vertical velocities that deform the wake and change its shape. This mechanism has been explained in the literature as a collection of vortices shed from the rotor plane (Howland et al., 2016; Bastankhah and Porté-Agel, 2016; Shapiro et al., 2018; Martínez-Tossas et al., 2019). The curled wake is a unique phenomenon in wind turbine wakes because it disrupts the asymmetry of the wake. The curled wake cannot be characterized by a symmetric profile such as a Gaussian distribution and requires a different modeling approach. The curled wake is known to affect not only a turbine immediately downstream, but also subsequent turbines within a wind plant. This effect is known as secondary steering and it is important to capture it when using wake models to unravel the full potential of wake steering (Fleming et al., 2018a; Bay et al., 2020; King et al., 2020).

The curled wake model uses a simplified version of the RANS equations to predict the wake of a wind turbine in yaw (Martínez-Tossas et al., 2019). Several improvements have been proposed to the original formulation of the model, including: 1) a decay model for the vortices, 2) tuning of the viscous term based on turbulence intensity, and 3) adding a pressure gradient term to account for wake expansion (Bay et al., 2019; Bay et al., 2020; Hulsman et al., 2020). Also, the new Gauss-Curl Hybrid model has shown to provide a good compromise between an analytical model (Bastankhah and Porté-Agel, 2016) and some of the physics from the curled wake model (King et al., 2020). The original formulation of the curled wake model was for a single wind turbine wake. In the case of a wind plant, the wakes are first computed individually, then superposed to obtain the flow field of the entire wind plant (Bay et al., 2020). Most wake models are used in the same manner by first computing the wake of the individual turbines and using a superposition method afterward to obtain the flow over the entire domain (Annoni et al., 2018). This new curled wake solver overcomes the use of a superposition method by solving the flow over the entire wind plant. This allows us to realize the benefits of the curled wake model in a much faster time frame with better scaling.

2 Formulation

We use the RANS equations to model the time-averaged flow field through a wind plant. The RANS equation for the streamwise
direction is:

$$\overline{u}\frac{\partial \overline{u}}{\partial x} + \overline{v}\frac{\partial \overline{u}}{\partial y} + \overline{w}\frac{\partial \overline{u}}{\partial z} = -\frac{1}{\rho}\frac{\partial \overline{p}}{\partial x} + \frac{\partial \overline{u'u'}}{\partial x} + \frac{\partial \overline{u'v'}}{\partial y} + \frac{\partial \overline{u'w'}}{\partial z} + \nu\left(\frac{\partial^2 \overline{u}}{\partial x^2} + \frac{\partial^2 \overline{u}}{\partial y^2} + \frac{\partial^2 \overline{u}}{\partial z^2}\right),$$ (1)

where x is the streamwise direction; y is the spanwise direction; z is the wall-normal direction; u, v and w are the velocity
components in the respective directions (with $'$ denoting time fluctuations and the overbar is time averaging); p is the time-
averaged pressure; and ρ is density. This is the same equation used in the original formulation of the curled wake model, but
now we focus on a new approach to derive the equations and some generalizations used for a wind plant approach as opposed
to a single wind turbine wake.

2.1 Decomposing the velocity

The velocity is decomposed into a background flow (capital letters) and a wake deficit (Δ) by:

$$u = U + \Delta u, \qquad v = V + \Delta v, \qquad w = W + \Delta w, \qquad p = P + \Delta p.$$ (2)

The time-averaged fields are denoted using overbars:

$$\overline{u} = \overline{U} + \overline{\Delta u}, \qquad \overline{v} = \overline{V} + \overline{\Delta v}, \qquad \overline{w} = \overline{W} + \overline{\Delta w}, \qquad \overline{p} = \overline{P} + \overline{\Delta p}.$$ (3)

The temporal fluctuations are denoted using a hash mark ($'$):

$$u' = U' + \Delta u', \qquad v' = V' + \Delta v', \qquad w' = W' + \Delta w', \qquad p' = P' + \Delta p'.$$ (4)

2.1.1 Background flow

The background flow (U, V, W) is the velocity of the domain where the wind turbines would be without including the wind
turbines and their wakes. The background flow formulation can be obtained from an analytical formulation such as the log-
law or from a different time-averaged simulation. For example, you can specify uniform flow by $U, V, W = U_\infty, 0, 0$, or use
simulation data from LES or experiments to define the background flow over complex terrain.

2.1.2 Wake deficit solution

The time-averaged wake velocities are denoted by $\overline{\Delta u}$, $\overline{\Delta v}$, and $\overline{\Delta w}$. We are interested in solving the streamwise component of
the wake deficit, $\overline{\Delta u}$, while the other wake velocity components, $\overline{\Delta v}$ and $\overline{\Delta w}$, are parametrized using semianalytical models.
The streamwise component of the RANS equations can be written in terms of the background flow and wake velocity as:

$$(\overline{U} + \overline{\Delta u})\frac{\partial(\overline{\Delta u} + \overline{U})}{\partial x} + (\overline{V} + \overline{\Delta v})\frac{\partial(\overline{U} + \overline{\Delta u})}{\partial y} + (\overline{W} + \overline{\Delta w})\frac{\partial(\overline{U} + \overline{\Delta u})}{\partial z} = -\frac{1}{\rho}\frac{\partial(P + p_{\mathrm{w}})}{\partial x}$$

$$+ \frac{\partial\overline{(U' + \Delta u')(U' + \Delta u')}}{\partial x} + \frac{\partial\overline{(U' + \Delta u')(V' + \Delta v')}}{\partial y} + \frac{\partial\overline{(U' + \Delta u')(W' + \Delta w')}}{\partial z}.$$ (5)

The background flow is defined to also satisfy the RANS equations as

$$85 \quad \overline{U}\frac{\partial \overline{U}}{\partial x} + \overline{V}\frac{\partial \overline{U}}{\partial y} + \overline{W}\frac{\partial \overline{U}}{\partial z} = -\frac{1}{\rho}\frac{\partial P}{\partial x} + \frac{\partial \overline{U'U'}}{\partial x} + \frac{\partial \overline{U'V'}}{\partial y} + \frac{\partial \overline{U'W'}}{\partial z}. \tag{6}$$

Subtracting the background flow (Equation 6) from the full flow (Equation 5) leads to the equation of the curled wake model:

$$(\overline{U}+\overline{\Delta u})\frac{\partial \overline{\Delta u}}{\partial x} + (\overline{V}+\overline{\Delta v})\frac{\partial \overline{\Delta u}}{\partial y} + (\overline{W}+\overline{\Delta w})\frac{\partial \overline{\Delta u}}{\partial z} + \overline{\Delta u}\frac{\partial \overline{U}}{\partial x} + \overline{\Delta v}\frac{\partial \overline{U}}{\partial y} + \overline{\Delta w}\frac{\partial \overline{U}}{\partial z} = -\frac{1}{\rho}\frac{\partial p_{\mathrm{w}}}{\partial x}$$
$$+ \frac{\partial \overline{(2U'\Delta u' + \Delta u'\Delta u')}}{\partial x} + \frac{\partial \overline{(U'\Delta v' + V'\Delta v' + \Delta u'\Delta v')}}{\partial y} + \frac{\partial \overline{(U'\Delta w' + W'\Delta u' + \Delta u'\Delta w')}}{\partial z}. \tag{7}$$

We now assume that the pressure gradient has a small effect (especially in the far wake). The Reynolds stresses are modeled as
90 a viscous term using a mixing length model and are dominated by spanwise gradients (Pope, 2000). The gradients of the mean
flow are assumed to be small, and their influence on the convective terms is neglected:

$$\overline{\Delta u}\frac{\partial \overline{U}}{\partial x} + \overline{\Delta v}\frac{\partial \overline{U}}{\partial y} + \overline{\Delta w}\frac{\partial \overline{U}}{\partial z} \ll (\overline{U}+\overline{\Delta u})\frac{\partial \overline{\Delta u}}{\partial x} + (\overline{V}+\overline{\Delta v})\frac{\partial \overline{\Delta u}}{\partial y} + (\overline{W}+\overline{\Delta w})\frac{\partial \overline{\Delta u}}{\partial z}. \tag{8}$$

This leads to the final form of the equation:

$$\boxed{\frac{\partial \overline{\Delta u}}{\partial x} = -\frac{1}{\overline{U}+\overline{\Delta u}}\left[(\overline{V}+\overline{\Delta v})\frac{\partial \overline{\Delta u}}{\partial y} + (\overline{W}+\overline{\Delta w})\frac{\partial \overline{\Delta u}}{\partial z} + \nu_{\mathrm{eff}}\left(\frac{\partial^2 \overline{\Delta u}}{\partial y^2} + \frac{\partial^2 \overline{\Delta u}}{\partial z^2}\right)\right].} \tag{9}$$

95 Equation 9 is the fundamental parabolic equation solved in the model presented. The streamwise velocity deficit, Δu, is the
main unknown; all the other variables in the equation are either known a priori or parametrized at run-time depending on Δu.
The equation is solved by marching in the downstream direction starting from an initial condition where the first wind turbine
is (section 3).

2.2 Turbulence model

100 The effect of turbulence in the RANS equations is described by the divergence of the Reynolds stress tensor. The streamwise
component of the divergence of the Reynolds stress for the background flow solution (Equation 6) is:

$$\frac{\partial \overline{U'U'}}{\partial x} + \frac{\partial \overline{U'V'}}{\partial y} + \frac{\partial \overline{U'W'}}{\partial z}. \tag{10}$$

The Reynolds stress term in Equation 7 (for the wake deficit solution) is defined as:

$$\frac{\partial \overline{(2U'\Delta u' + \Delta u'\Delta u')}}{\partial x} + \frac{\partial \overline{(U'\Delta v' + V'\Delta v' + \Delta u'\Delta v')}}{\partial y} + \frac{\partial \overline{(U'\Delta w' + W'\Delta u' + \Delta u'\Delta w')}}{\partial z}. \tag{11}$$

105 The decomposition of the velocity field (background + wake, mean + fluctuation) leads to the introduction of additional stress-
like terms in Equation 7. These terms are correlations between the background flow solution and the wake deficit solution.
These terms need to be taken into account when solving Equation 7.

A mixing length model is used to represent the terms in Equation 11. We propose using the simple model suggested in the
original formulation of the curled wake model (Martínez-Tossas et al., 2019) and scale the viscosity to take into account the

effect from all of the extra terms in the Reynolds stresses from Equation 11. This is the same approach suggested by Bay et al. (2019). The mixing length and turbulent viscosity are defined as:

$$\ell_{\mathrm{m}} = \frac{\kappa z}{(1 + \kappa z / \lambda)} \qquad \nu_{\mathrm{eff}} = C \, \ell_{\mathrm{m}}^2 \left| \frac{d\overline{U}}{dz} \right| \tag{12}$$

where ℓ_{m} is the mixing length, ν_{eff} is the turbulent viscosity, κ is the von Kármán constant, z is the distance from the ground, $\lambda = 15\mathrm{m}$ is the value of the mixing length in the free atmosphere. and C is a scaling constant (Blackadar, 1962; Sun, 2011). The constant C is used to take into account all of the extra terms in Equation 11. Testing from Bay et al. (2020) has shown that for all of the cases tried in the manuscript, a value of $C = 8$ has provided good agreement between the model and experiments/simulations. This value is consistent with what is suggested by Bay et al. (2019). The mixing length and turbulent viscosity are difficult to approximate with constant values that depend only on height (z). A better approximation would allow turbulent viscosity to vary spatially, especially in the wake, where the local turbulence varies with the spanwise and streamwise coordinates. The model presented aims to simplify the turbulent viscosity; properly resolving these terms would require a different and more complex approach (van der Laan et al., 2015; Iungo et al., 2018).

2.3 Wind turbine wakes initial condition

Wakes are initialized according to the wind speed at the rotor location in the plane closest to where the turbine is. As the solution marches downstream and new wind turbines are encountered, a new wake deficit is added to the plane with a diameter including the expansion of the wake:

$$\overline{\Delta u} = -2\,a\,\langle \overline{U} + \overline{\Delta u} \rangle \tag{13}$$

where $a = (1 - \sqrt{1 - C_T})/2$ is the induction from momentum theory, C_T is the thrust coefficient, and $< \overline{U} + \overline{\Delta u} >$ is the averaged velocity inside the disk. A Gaussian filter is used to smear the initial condition in the spanwise directions to avoid numerical instabilities described in Martínez-Tossas et al. (2019). The effects of wake curl, wake rotation, and the boundary layer are implemented using the analytical models also described in Martínez-Tossas et al. (2019). For completeness, we show the analytical formulas for the spanwise velocities from the curled wake. The effect of curl is added by modifying the spanwise velocity components according to an elliptic distribution of vorticity (Shapiro et al., 2018; Martínez-Tossas et al., 2019; Martínez-Tossas and Branlard, 2020). The spanwise velocities can be represented analytically by:

$$v' = \int\limits_{-R}^{R} \frac{(z - z')}{2\pi \left(y^2 + (z - z')^2 \right)} \left(1 - e^{-(y^2 + (z-z')^2)/\sigma^2} \right) \Gamma_0 \frac{z'}{R\sqrt{R^2 - z'^2}} dz' \tag{14}$$

$$w' = \int\limits_{-R}^{R} \frac{-y}{2\pi \left(y^2 + (z - z')^2 \right)} \left(1 - e^{-(y^2 + (z-z')^2)/\sigma^2} \right) \Gamma_0 \frac{z'}{R\sqrt{R^2 - z'^2}} dz'. \tag{15}$$

where R is the turbine radius, y and z are the coordinates relative to the disk center, and $\Gamma_0 = \frac{D}{2} C_T \, U_\infty \sin\alpha \cos^2\alpha$ is the total circulation from yaw (Shapiro et al., 2018; Martínez-Tossas et al., 2019).

3 Numerical Solution

It is now possible to write Equation 1 using numerical differentiation. Equation 16 shows the equation to be solved numerically
140 with all of the terms labeled that are to be discretized:

$$
\overline{\Delta u}_{[i+1,j,k]} = \overline{\Delta u}_{[i,j,k]} - \overbrace{\frac{\Delta x}{\overline{U} + \overline{\Delta u}}}^{A} \left[\overbrace{(\overline{V} + \overline{\Delta v})\frac{\partial \overline{\Delta u}}{\partial y}}^{B} + \overbrace{(\overline{W} + \overline{\Delta w})\frac{\partial \overline{\Delta u}}{\partial z}}^{C} + \nu_{\text{eff}} \left(\overbrace{\frac{\partial^2 \overline{\Delta u}}{\partial y^2}}^{D} + \overbrace{\frac{\partial^2 \overline{\Delta u}}{\partial z^2}}^{E} \right) \right]. \tag{16}
$$

The terms in Equation 16 can be defined discretely as:

$$
B + C \rightarrow \left(\overline{V}_{[i,j,k]} + \overline{\Delta v}_{[i,j,k]} \right) \frac{\overline{\Delta u}_{[i,j+1,k]} - \overline{\Delta u}_{[i,j-1,k]}}{\Delta y} + \left(\overline{W}_{[i,j,k]} + \overline{\Delta w}_{[i,j,k]} \right) \frac{\overline{\Delta u}_{[i,j,k+1]} - \overline{\Delta u}_{[i,j,k-1]}}{\Delta z}
$$

$$
D + E \rightarrow \frac{\overline{\Delta u}_{[i,j+1,k]} - 2\overline{\Delta u}_{[i,j,k]} + \overline{\Delta u}_{[i,j-1,k]}}{\Delta y^2} + \frac{\overline{\Delta u}_{[i,j,k+1]} - 2\overline{\Delta u}_{[i,j,k]} + \overline{\Delta u}_{[i,j,k-1]}}{\Delta z^2}. \tag{17}
$$

145 This numerical equation is discretized using a forward-in-time, centered-in-space formulation with the stability criteria shown
in Equation 18 (Hoffman and Frankel, 2018; Martínez-Tossas et al., 2019). We note that the model proposed is steady stated and
there is no time dependency. The spatial streamwise direction is treated as the 'forward-in-time' part of the numerical method.
The equations can be solved as a marching problem in the streamwise direction (index i) starting with an initial condition in a
yz plane. The boundary conditions are set to zero wake deficit ($\overline{\Delta u} = 0$):

150 $$
\Delta x \leq 2\nu_{\text{eff}} \frac{\overline{\Delta u}}{(\overline{W} + \overline{\Delta w})^2}, \quad \Delta y \geq \sqrt{2\nu_{\text{eff}} \Delta x / \overline{\Delta u}}. \tag{18}
$$

Our tests have shown that the implementation has a converged and stable solution when using a grid resolution on the order of
$\frac{D}{\Delta y}$10-20 in the spanwise directions (y and z) and $\frac{D}{\Delta x}$30-40 in the streamwise direction.

Figure 1 shows a schematic of how the solution is computed. The main figure is a contour of streamwise velocity from a
simulation with a random arrangement of turbines. The solution is marched downstream by solving Equation 16 at each plane.
155 Two planes are shown from the middle of the domain. The final solution includes a collection of planes for each streamwise
location, which are combined to generate a full 3D solution.

3.1 Computational cost

To better understand the low computational cost of the solver presented, we asses the number of floating point operations
needed to obtain a solution to 15. We estimate the computational expense of the implementation by approximating the number
160 of floating point operations (summation, subtraction, multiplication, division) in each term in Equation 16. We assume that
the total number of grid points in the computational domain is N. To solve Equation 16, all the grid points in the domain
must compute each of the terms in the equation. This leads to the following computational expense from each term: $A = 2N$, $B = 4N$, $C = 4N$, $D = 5N$, $E = 5N$ and, assuming one floating point operation between terms ($4N$), this leads to a
total computational expense of $\approx 24N$ floating point operations. Assuming that we use a standard processor ($1-$Gflops), the
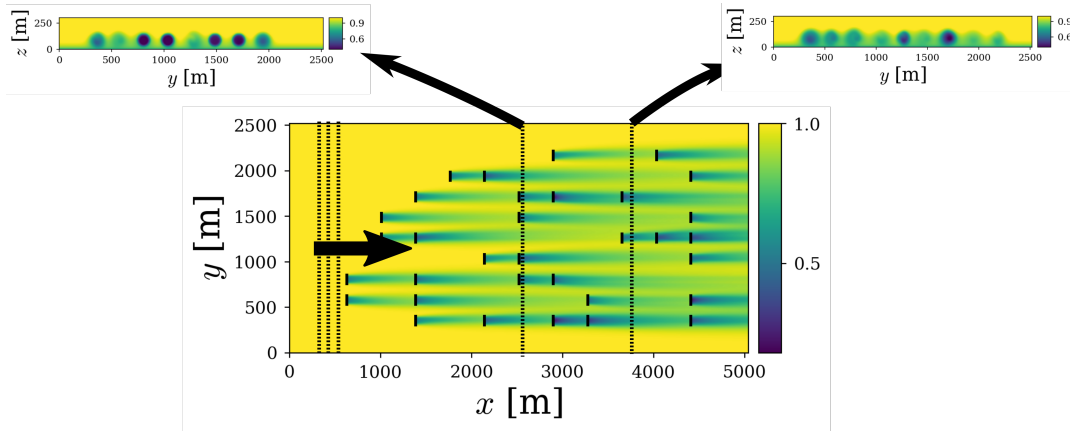
Figure 1. Schematic of the computational strategy used to solve equation 16. Dashed lines denote the location of a subset of planes, and big arrow shows the marching direction.

computational time required for a simulation with $N = 100^3$ grid points based on this approximation would be .02 [s]. This can be considered an extremely fast solver for wind plant controls and layout optimization. In practice, the computational expense of the algorithm heavily depends on the implementation and software stack used. In our current implementation within the numpy and python frameworks (van der Walt et al., 2011), the typical computational cost of a simulation is on the order of 0.1-10 seconds. This is two order of magnitude faster than the standard curl model implementation in the FLOw Redirection and Induction in Steady State (FLORIS) framework. Figure 2 shows the time to solution of the algorithm as a function of total number of grid points from the model presented compared to the standard FLORIS implementation with wake superposition (Bay et al., 2019) compared to the linear scaling of the new solver. Also, the wind plant used for the scaling study is shown for reference. The resolutions used are finer than required for this wind plant, and the simulations lasting 0.5 seconds are converged and would be used for production runs.

4 Results

We use the model proposed to compare with three different cases. The first comparison is done using SCADA from the Lillgrund wind plant. Second, we showcase the use of the solver in complex terrain. Finally, we compare the model to a series of LES for an array of turbines with different yaw combinations.

4.1 Lillgrund Wind Plant

We use the model proposed to compute the flow field over the Lillgrund Wind Plant. Ten-minute average SCADA is available for all turbines for different wind conditions. Three conditions from directions where the meteorological tower is not waked were chosen (185° with 41 10-minute averages, 215° with 93 10-minute averages, and 255° with 90 10-minute averages). For each wind condition, we perform one simulation with the solver proposed. Figure 3 shows the layout of the Lillgrund Wind
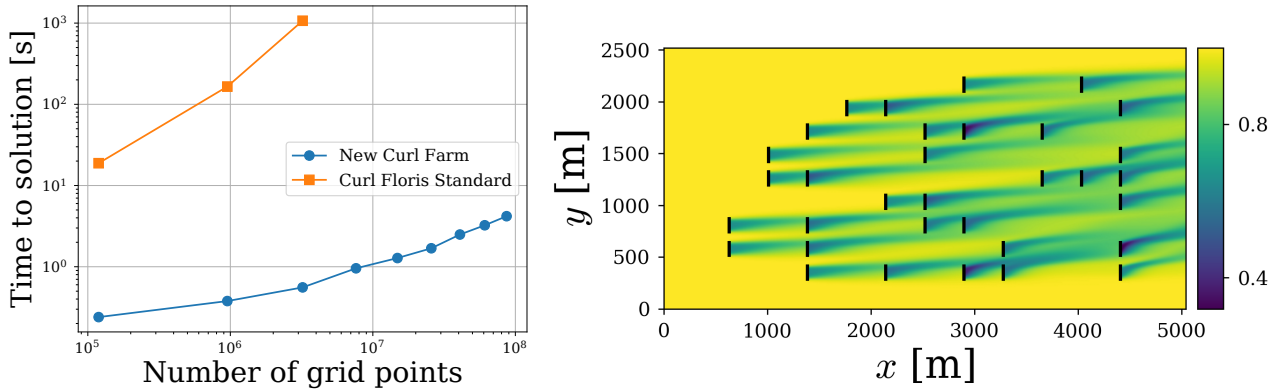
Figure 2. Scaling of the computational algorithm (left) based on a representative wind plant composed of 36 turbines with wake steering (right).

Plant with arrows denoting the directions for the cases that were studied. The background flow was set to a log-law streamwise velocity profile with a roughness height of $z_0 = 10^{-5}$[m].
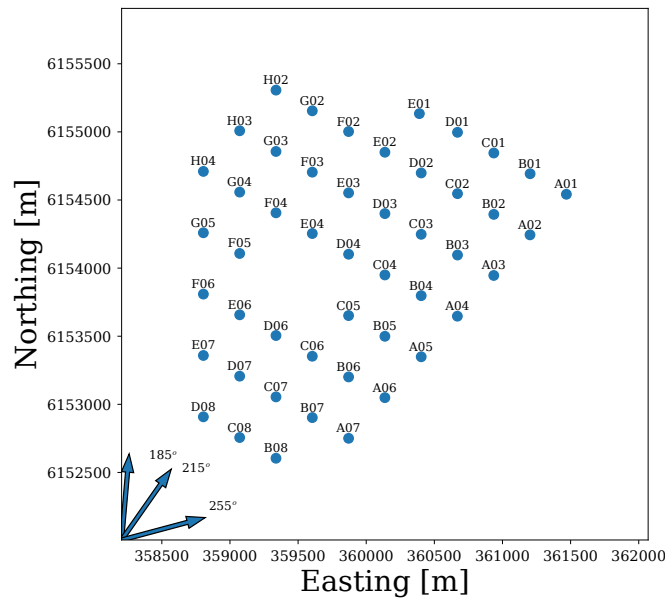
Figure 3. Layout of the Lillgrund Wind Plant with wind direction used in each simulation.

Figure 4 shows a comparison of power output between the SCADA and the model proposed with a streamwise velocity contour at hub height. The data has been normalized according to the highest mean power in the experimental data. The bars in the SCADA indicate the standard deviation of the power measurements. The agreement between the SCADA and the model is excellent, with most results from the proposed solver lying within one standard deviation of the measurements. We can see

190 different features of the flow, including the superposition of wakes. The solver computes the power and thrust from each turbine according to the local velocity. This allows for the solver to reach an equilibrium state in the deep array region. In this area, the power produced by the turbine flattens; it is a balance between the turbulent diffusion and the power extraction.
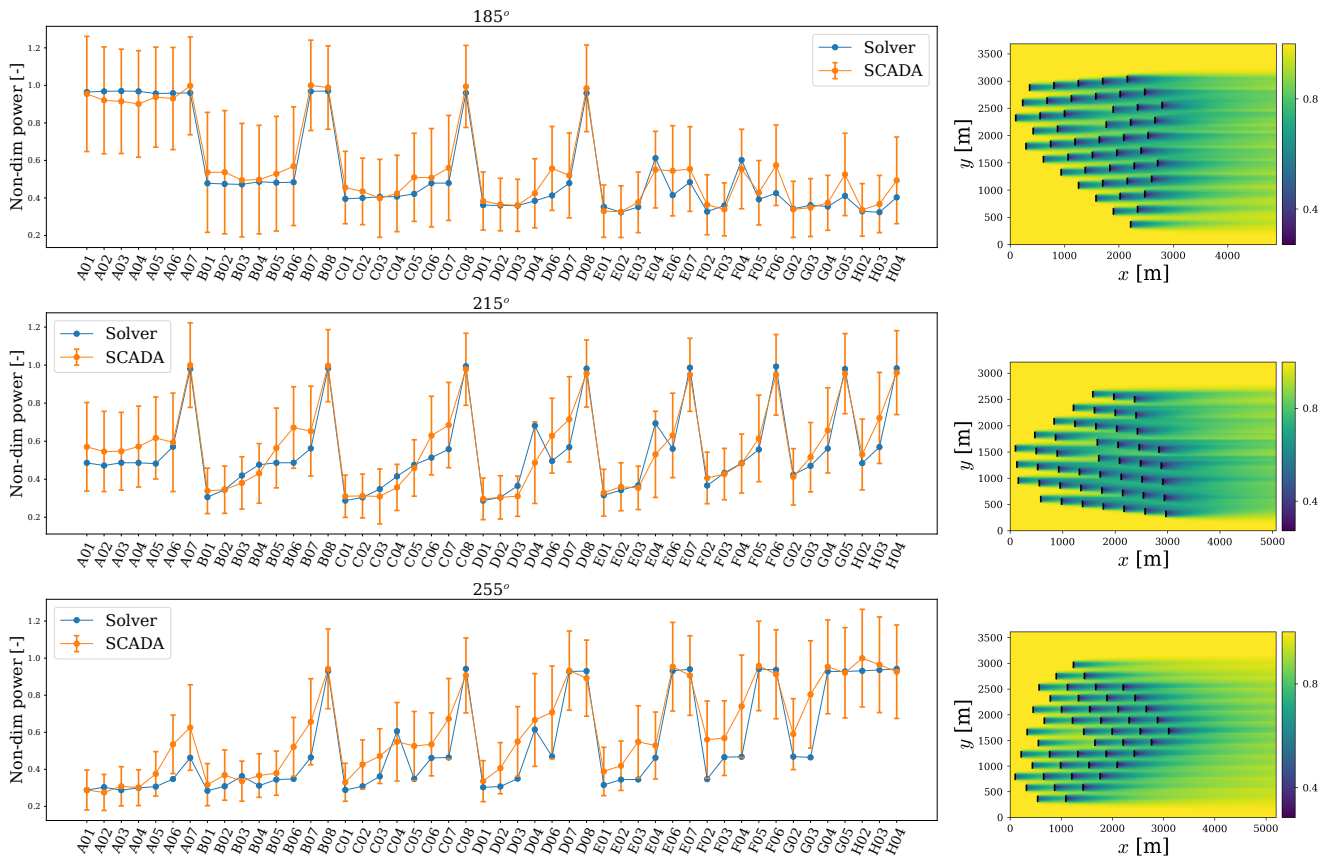
Figure 4. Comparison of turbine power versus SCADA for the Lillgrund Wind Plant for cases at three different wind directions (185°, 215°, 255°). Streamwise velocity contours at hub height are shown for all cases with the wind plant aligned with the flow direction.

4.2 Complex terrain: Columbia River Gorge

We test the model presented on a case with complex terrain over the Columbia River Gorge (Quon et al., 2019). This test
195 case is used to demonstrate the capabilities of the model in complex terrain conditions. The background flow solution is taken from a time-averaged LES (Quon et al., 2019). Figure 5 shows a volume rendering of streamwise velocity from a simulation using the proposed model. We can see the three-dimensionality of the solution and how the wakes conform to the terrain. The background flow is taken from LES, and the algorithm provides the solution for the wake deficits that would be present if turbines were there. Figure 6 shows streamwise velocity contours for planes in all directions. It is interesting to see how the
200 wakes advect sideways following the background flow. Also, the combination of wakes leads to asymmetric deformation not

typically observed in wakes over flat terrain. These results serve as a test case to show the applicability of the model in a case with complex terrain; further work is needed to assess the accuracy of the model under complex terrain conditions.
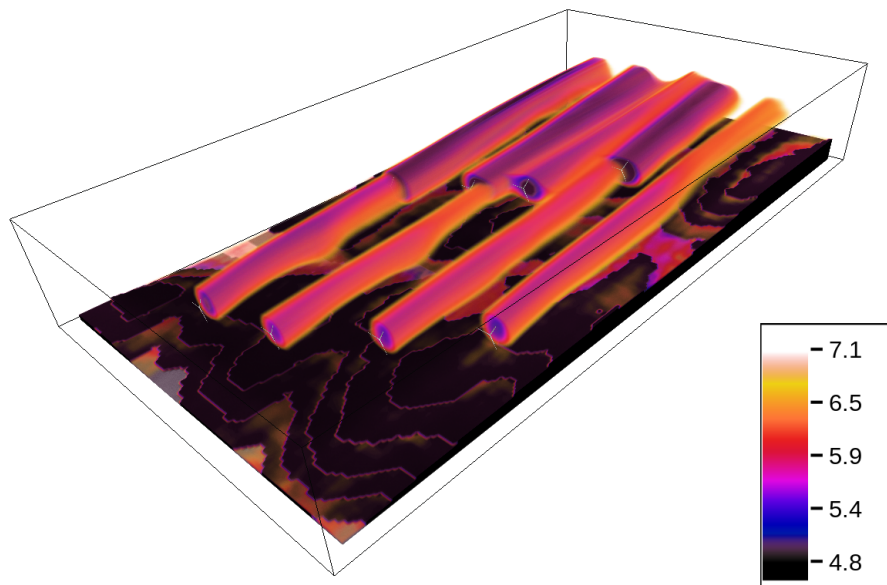
Figure 5. Volume rendering of streamwise velocity from a simulation using the proposed model. Image produced using Vapor (Li et al., 2019).
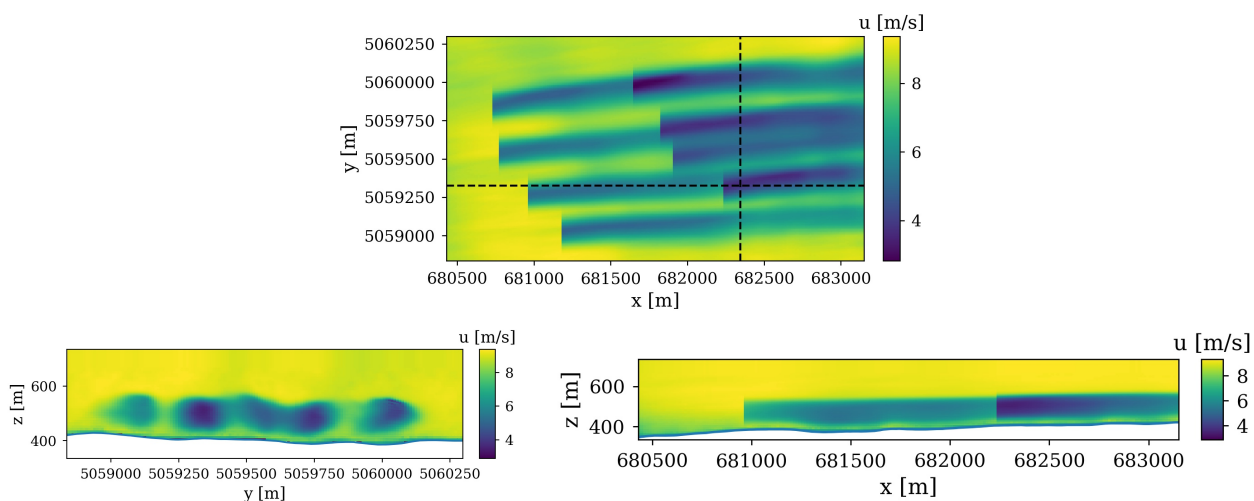
Figure 6. Streamwise velocity contours showing a plane perpendicular to the wall-normal direction (top) and the streamwise direction (bottom). The horizontal and vertical lines denote the location of the planes.

4.3 Wake steering

We now compare the model to results from LES of wakes in steering conditions. The simulations were performed using the
205 Simulator fOr Applications (SOWFA) using an actuator disk model with rotation (Churchfield et al., 2012). The simulations are
for cases with wind plants of 4-by-3 and 3-by-3 turbines with different offsets and yaw-angle combinations. The simulations
use a precursor simulation from a neutral atmospheric boundary layer with roughness height of $z_0 = 0.15$[m] and wind speed
at hub height (90[m]) of 8 [m/s]. The simulations are time-averaged over 1,600 [s]. Table 1 shows the main parameters for the
simulations.

210 Figure 7 shows the total power for each case from the model proposed and from LES. There is good agreement in total
power between the model and the simulations. The model proposed is able to capture the effects of yaw and general trends of
power output from the different configurations. We note that the simulations still have some transient effects and differences
arise from transient effects in the atmospheric boundary layer, including low-velocity streaks passing through the turbines.

Case	Number of Turbines	Hub-height velocity	Turbulence Intensity	Yaw Angles [^{o}]
0	12	8 [m/s]	10.0 %	-20, -20, -20, -20, 0, 0, 0, 0, 0, 0, 0, 0,
1	12	8 [m/s]	10.0 %	0, 0, 0, 0, 0, 0, 0, 0, 0, 0, 0, 0,
2	12	8 [m/s]	10.0 %	5, 10, 15, 20, 0, 0, 0, 0, 0, 0, 0, 0,
3	12	8 [m/s]	10.0 %	10, 10, 10, 10, 0, 0, 0, 0, 0, 0, 0, 0,
4	12	8 [m/s]	10.0 %	20, 15, 10, 5, 0, 0, 0, 0, 0, 0, 0, 0,
5	12	8 [m/s]	10.0 %	20, 20, 20, 20, 0, 0, 0, 0, 0, 0, 0, 0,
6	12	8 [m/s]	10.0 %	20, 20, 20, 20, 10, 10, 10, 10, 0, 0, 0, 0,
7	9	8 [m/s]	10.0 %	-20, -20, -20, 0, 0, 0, 0, 0, 0,
8	9	8 [m/s]	10.0 %	0, 0, 0, 0, 0, 0, 0, 0, 0,
9	9	8 [m/s]	10.0 %	10, 10, 10, 0, 0, 0, 0, 0, 0,
10	9	8 [m/s]	10.0 %	20, 20, 20, 0, 0, 0, 0, 0, 0,
11	9	8 [m/s]	10.0 %	20, 20, 20, 10, 10, 10, 0, 0, 0,

Table 1. List of LES cases performed for comparison study.
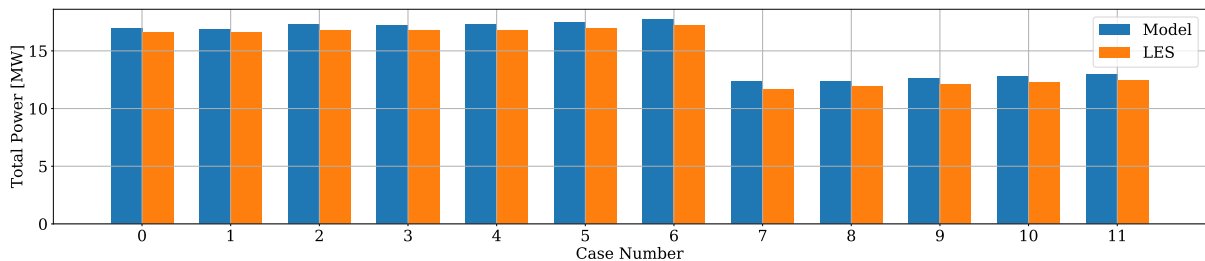
Figure 7. Total power output for wind plant LES with wake steering compared with the model proposed.

We select two cases and show the power for all turbines and a plane at hub height with wake profiles from the model
proposed. Figure 8 shows power for all turbines and a velocity profile at hub height for cases 2 and 6. There is good agreement
between the model and the LES. The unsteadiness in the atmospheric boundary layer inflow creates some of the differences in
turbine power. These differences are expected to diminish with longer time averaging. Also, we observed consistent differences
in the power output of turbines further donwstream. These differences are caused by the lack of a more sophisticated turbulence
model that can take into account the wake-added turbulence. We are currently working on improving the turbulence model and
incorporating some of the findings from (Bay et al., 2019).
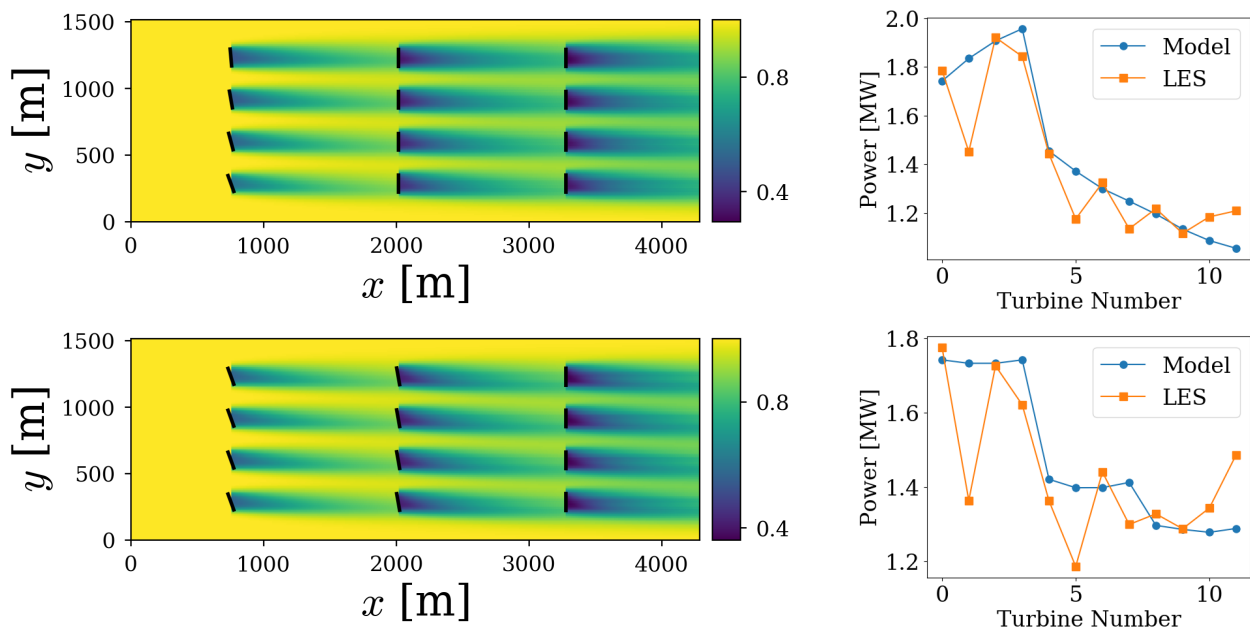
Figure 8. Velocity at hub height from the model proposed and the power output for each turbine from the model proposed compared to
results from LES.

5 Conclusions

Fast wind power plant flow solvers are much needed for wind plant controls and layout optimization. In this work, we presented
a simplified and fast solver for wind turbine wakes based on the curled wake model presented in Martínez-Tossas et al. (2019).
This solver is based on a parabolic equation for the streamwise component of the Reynolds-averaged Navier-Stokes equation.
The computational expense was shown to be on the order of seconds for a full wind plant with 36 turbines. The model was tested
on three different cases: 1) SCADA from the Lillgrund Wind Plant 2) LES for flow over complex terrain, and 3) LES over flat
terrain with different yaw-angle combinations. The models showed good agreement with the SCADA from the Lillgrund Wind
Plant. The model was also able to generate wake profiles for data in complex terrain and future work will focus on comparing
these profiles to data. Finally, the solver was able to reproduce the trends from LES with different yaw combinations. The

model presented was shown to be an extremely fast solver (order of seconds) for wind turbine wakes with terrain features. This was achieved by simplifying the streamwise component of the RANS equation and making a series of assumptions. This model uses many simplifications, especially with regard to the turbulence model,to improve computational speed. This trade-off provides a very computationally efficient solver at the expense of less robust turbulence modeling. This solver will soon be incorporated into the FLORIS framework and will be freely available. Future work will consist of implementing a vortex decay model and using the solver for yaw-angle optimizations in a wind plant.

Code availability. The code will soon be available withing the FLORIS framework.

Author contributions. LAMT led the model development and writing the article. All authors provided input to this manuscript.

Competing interests. No competing interest.

6 Acknowledgments

The authors would like to thank Paula Doubrawa for help in allocating funding for this work and Sheri Anstedt from NREL for their help in editing the manuscript. Data was furnished to the authors under an agreement between the National Renewable Energy Laboratory, Siemens Gamesa Renewable Energy A/S, and Vattenfall. Data and results used herein do not reflect findings by Siemens Gamesa Renewable Energy A/S and Vattenfall. A portion of the research was performed using computational resources sponsored by the U.S. Department of Energy's Office of Energy Efficiency and Renewable Energy and located at the National Renewable Energy Laboratory. This work was authored by the National Renewable Energy Laboratory, operated by Alliance for Sustainable Energy, LLC, for the U.S. Department of Energy (DOE) under Contract No. DE-AC36-08GO28308. Funding provided by the U.S. Department of Energy Office of Energy Efficiency and Renewable Energy Wind Energy Technologies Office. The views expressed in the article do not necessarily represent the views of the DOE or the U.S. Government. The U.S. Government retains and the publisher, by accepting the article for publication, acknowledges that the U.S. Government retains a nonexclusive, paid-up, irrevocable, worldwide license to publish or reproduce the published form of this work, or allow others to do so, for U.S. Government purposes.

References

Adaramola, M. and Krogstad, P.-A.: Experimental investigation of wake effects on wind turbine performance, Renewable Energy, 36, 2078 – 2086, 2011.

Annoni, J., Fleming, P., Scholbrock, A., Roadman, J., Dana, S., Adcock, C., Porte-Agel, F., Raach, S., Haizmann, F., and Schlipf, D.: Analysis of control-oriented wake modeling tools using lidar field results, Wind Energy Science, 3, 819–831, https://doi.org/10.5194/wes-3-819-2018, https://www.wind-energ-sci.net/3/819/2018/, 2018.

Bartl, J., Mühle, F., Schottler, J., Saetran, L., Peinke, J., Adaramola, M., and Hölling, M.: Wind tunnel experiments on wind turbine wakes in yaw: effects of inflow turbulence and shear, Wind Energy Science, 3, 329–343, https://doi.org/10.5194/wes-3-329-2018, 2018.

Bastankhah, M. and Porté-Agel, F.: Experimental and theoretical study of wind turbine wakes in yawed conditions, Journal of Fluid Mechanics, 806, 506–541, https://doi.org/10.1017/jfm.2016.595, 2016.

Bay, C. J., Annoni, J., Martínez-Tossas, L. A., Pao, L. Y., and Johnson, K. E.: Flow Control Leveraging Downwind Rotors for Improved Wind Power Plant Operation, in: 2019 American Control Conference (ACC), pp. 2843–2848, 2019.

Bay, C. J., King, J., Martínez-Tossas, L. A., Mudafort, R., Hulsman, P., Kühn, M., and Fleming, P.: Towards flow control: an assessment of the curled wake model in the FLORIS framework, in: Submitted to Torque 2020, 2020.

Blackadar, A. K.: The vertical distribution of wind and turbulent exchange in a neutral atmosphere, Journal of Geophysical Research, 67, 3095–3102, 1962.

Bradstock, P. and Schlez, W.: Theory and Verification of a new 3D RANS model, 2019a.

Bradstock, P. and Schlez, W.: Theory and Validation of a 3D RANS Wake Model, in: Wind Energy Science Conference, 2019b.

Churchfield, M., Lee, S., Moriarty, P., Martinez, L., Leonardi, S., Vijayakumar, G., and Brasseur, J.: A Large-Eddy Simulation of Wind-Plant Aerodynamics, in: 50th AIAA Aerospace Sciences Meeting including the New Horizons Forum and Aerospace Exposition, https://doi.org/10.2514/6.2012-537, https://arc.aiaa.org/doi/abs/10.2514/6.2012-537, 2012.

Fleming, P., Annoni, J., Churchfield, M., Martinez-Tossas, L. A., Gruchalla, K., Lawson, M., and Moriarty, P.: A simulation study demonstrating the importance of large-scale trailing vortices in wake steering, Wind Energy Science, 3, 243–255, https://doi.org/10.5194/wes-3-243-2018, https://www.wind-energ-sci.net/3/243/2018/, 2018a.

Fleming, P., Annoni, J., Martínez-Tossas, L. A., Raach, S., Gruchalla, K., Scholbrock, A., Churchfield, M., and Roadman, J.: Investigation into the shape of a wake of a yawed full-scale turbine, Journal of Physics: Conference Series, 1037, 032 010, 2018b.

Fleming, P., King, J., Dykes, K., Simley, E., Roadman, J., Scholbrock, A., Murphy, P., Lundquist, J. K., Moriarty, P., Fleming, K., van Dam, J., Bay, C., Mudafort, R., Lopez, H., Skopek, J., Scott, M., Ryan, B., Guernsey, C., and Brake, D.: Initial results from a field campaign of wake steering applied at a commercial wind farm – Part 1, Wind Energy Science, 4, 273–285, https://doi.org/10.5194/wes-4-273-2019, https://www.wind-energ-sci.net/4/273/2019/, 2019.

Gebraad, P. M. O., Teeuwisse, F. W., van Wingerden, J. W., Fleming, P. A., Ruben, S. D., Marden, J. R., and Pao, L. Y.: Wind plant power optimization through yaw control using a parametric model for wake effects?a CFD simulation study, Wind Energy, 19, 95–114, we.1822, 2016.

Gunn, K., Stock-Williams, C., Burke, M., Willden, R., Vogel, C., Hunter, W., Stallard, T., Robinson, N., and Schmidt, S. R.: Limitations to the validity of single wake superposition in wind farm yield assessment, Journal of Physics: Conference Series, 749, 012 003, https://doi.org/10.1088/1742-6596/749/1/012003, 2016.

Hoffman, J. and Frankel, S.: Numerical Methods for Engineers and Scientists, CRC Press, https://books.google.com/books?id=
F5K3DwAAQBAJ, 2018.

290 Howland, M. F., Bossuyt, J., Martínez-Tossas, L. A., Meyers, J., and Meneveau, C.: Wake structure in actuator disk models of wind turbines
in yaw under uniform inflow conditions, Journal of Renewable and Sustainable Energy, 8, 043 301, https://doi.org/10.1063/1.4955091,
2016.

Howland, M. F., Lele, S. K., and Dabiri, J. O.: Wind farm power optimization through wake steering, Proceedings of the National Academy
of Sciences, 116, 14 495–14 500, https://doi.org/10.1073/pnas.1903680116, https://www.pnas.org/content/116/29/14495, 2019.

295 Hulsman, P., Martinez-Tossas, L. A., Hamilton, N., and Kuhn, M.: Modelling and assessing the near-wake representation and turbulence
behaviour of control-oriented wake models, Torque 2020: Accepted, 2020.

Iungo, G. V., Santhanagopalan, V., Ciri, U., Viola, F., Zhan, L., Rotea, M. A., and Leonardi, S.: Parabolic RANS solver for low-computational-
cost simulations of wind turbine wakes, Wind Energy, 21, 184–197, https://doi.org/10.1002/we.2154, https://onlinelibrary.wiley.com/doi/
abs/10.1002/we.2154, 2018.

300 King, J., Fleming, P., King, R., Martínez-Tossas, L. A., Bay, C. J., Mudafort, R., and Simley, E.: Controls-Oriented Model for Sec-
ondary Effects of Wake Steering, Wind Energy Science Discussions, 2020, 1–22, https://doi.org/10.5194/wes-2020-3, https://www.
wind-energ-sci-discuss.net/wes-2020-3/, 2020.

Li, S., Jaroszynski, S., Pearse, S., Orf, L., and Clyne, J.: VAPOR: A Visualization Package Tailored to Analyze Simulation Data in Earth
System Science, Atmosphere, 10, https://doi.org/10.3390/atmos10090488, https://www.mdpi.com/2073-4433/10/9/488, 2019.

305 Martínez-Tossas, L. A. and Branlard, E.: The curled wake model: equivalence of shed vorticity models, Journal of Physics: Confer-
ence Series, 1452, 012 069, https://doi.org/10.1088/1742-6596/1452/1/012069, https://doi.org/10.1088%2F1742-6596%2F1452%2F1%
2F012069, 2020.

Martínez-Tossas, L. A., Annoni, J., Fleming, P. A., and Churchfield, M. J.: The aerodynamics of the curled wake: a simplified model in view
of flow control, Wind Energy Science, 4, 127–138, https://doi.org/10.5194/wes-4-127-2019, https://www.wind-energ-sci.net/4/127/2019/,
310 2019.

Medici, D. and Alfredsson, P.: Measurements on a wind turbine wake: 3D effects and bluff body vortex shedding, Wind Energy, 9, 219–236,
2006.

Park, J., Kwon, S., and Law, K. H.: Wind farm power maximization based on a cooperative static game approach, in: Proc. SPIE, vol. 8688,
p. 86880R, 2013.

315 Pope, S. B.: Turbulent Flows, Cambridge University Press, https://doi.org/10.1017/CBO9780511840531, 2000.

Quon, E. W., Doubrawa, P., Annoni, J., Hamilton, N., and Churchfield, M. J.: Validation of Wind Power Plant Modeling Approaches in
Complex Terrain, in: AIAA Scitech 2019 Forum, https://doi.org/10.2514/6.2019-2085, https://arc.aiaa.org/doi/abs/10.2514/6.2019-2085,
2019.

Schottler, J., Bartl, J., Mühle, F., Sætran, L., Peinke, J., and Hölling, M.: Wind tunnel experiments on wind turbine wakes in yaw: redefining
320 the wake width, Wind Energy Science, 3, 257–273, https://doi.org/10.5194/wes-3-257-2018, https://www.wind-energ-sci.net/3/257/2018/,
2018.

Shapiro, C. R., Gayme, D. F., and Meneveau, C.: Modelling yawed wind turbine wakes: a lifting line approach, Journal of Fluid Mechanics,
841, R1, https://doi.org/10.1017/jfm.2018.75, 2018.

Siemens Gamesa: Siemens Gamesa now able to actively dictate wind flow at offshore wind locations, Press release, https://www.siemensgamesa.com/en-int/-/media/siemensgamesa/downloads/en/newsroom/2019/11/press-release-siemens-gamesa-wake-adapt-en.pdf, 2019.

Sun, J.: Vertical variations of mixing lengths under neutral and stable conditions during CASES-99, Journal of Applied Meteorology and Climatology, 50, 2030–2041, 2011.

van der Laan, M. P., Sorensen, N. N., Rethore, P.-E., Mann, J., Kelly, M. C., Troldborg, N., Schepers, J. G., and Machefaux, E.: An improved k-ϵ model applied to a wind turbine wake in atmospheric turbulence, Wind Energy, 18, 889–907, https://doi.org/10.1002/we.1736, 2015.

van der Walt, S., Colbert, S., and Varoquaux, G.: The NumPy Array: A Structure for Efficient Numerical Computation, Computing in Science & Engineering, 13, 22 – 30, https://doi.org/10.1109/MCSE.2011.37, 2011.

Vollmer, L., Steinfeld, G., Heinemann, D., and Kühn, M.: Estimating the wake deflection downstream of a wind turbine in different atmospheric stabilities: an LES study, Wind Energy Science, 1, 129–141, 2016.

Zong, H. and Porté-Agel, F.: A momentum-conserving wake superposition method for wind farm power prediction, Journal of Fluid Mechanics, 889, A8, https://doi.org/10.1017/jfm.2020.77, 2020.